Inorganic Chemistry

Article

pubs.acs.org/IC

Increasing the Dynamic Range of Metal Ion Affinity Changes in Zn^{2+} Photocages Using Multiple Nitrobenzyl Groups

Celina Gwizdala,[†] Prem N. Basa,[‡] John C. MacDonald,[‡] and Shawn C. Burdette*[,‡]

[‡]Department of Chemistry and Biochemistry, Worcester Polytechnic Institute, 100 Institute Road, Worcester, Massachusetts 01609-2280, United States

[†]Department of Chemistry, University of Connecticut, 55 North Eagleville Road U-3060, Storrs, Connecticut 06269, United States

Supporting Information

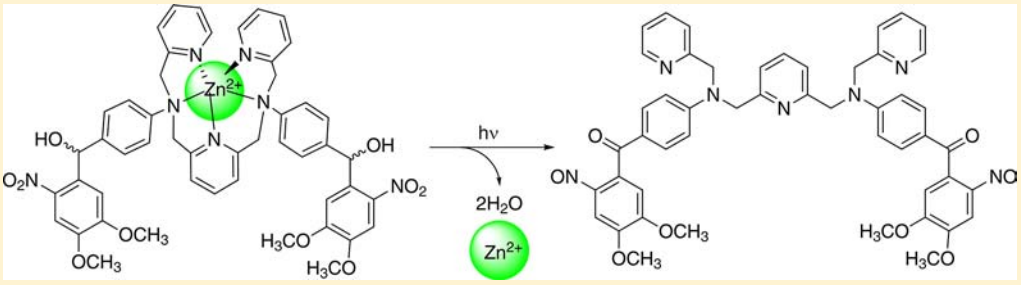

ABSTRACT: Two generations of DiCast photocages that exhibit light-induced decreases in metal ion affinity have been prepared and characterized. Expansion of the common Zn^{2+} chelator of *N*,*N*-dipicolylaniline (DPA) to include additional aniline ligand provides *N*,*N*′-diphenyl-*N*,*N*′-bis(pyridin-2-ylmethyl)ethane-1,2-diamine, a tetradentate ligand that was functionalized with two photolabile groups to afford DiCast-1. Uncaging of the nitrobenzhydrol reduces the electron density on two metal-bound aniline ligands, which decreases the Zn^{2+} affinity 190-fold. The analogous MonoCast photocage with a single nitrobenzhydrol group only undergoes a 14-fold reduction in affinity after an identical photochemical transformation. A second series of DiCast photocages based on a *N*,*N*′-(pyridine-2,6-diylbis(methylene))dianiline scaffold, which allows the introduction of two additional Zn^{2+}-binding ligands into a preorganized chelator, expand on the multi-photolabile group strategy. DiCast-2 includes two pyridine ligands while DiCast-3 adds two carboxylate groups. Addition of bridging pyridine to the second generation photocages leads to more stable Zn^{2+} complexes, and photolysis of two photolabile groups increases the Zn^{2+} affinity changes to 480-fold. The Zn^{2+}, Cu^{2+}, and Cd^{2+} binding properties were examined in all the DiCast photocages and the corresponding photoproducts using UV−vis spectroscopy. Further insight into the photocage Zn^{2+}-binding motifs was obtained by X-ray analysis of DiCast-2 and DiCast-3 model ligands.

INTRODUCTION

Photocages are indispensable tools for studying molecular biology.[1−3] The light-induced release of bioactive species allows time and delivery location to be controlled. Such photochemical tools permit quantitative manipulation of bioactive species with greater precision than alternative methods. While photocaged complexes have facilitated significant insight into Ca^{2+} signaling pathways,[2,4] other metal ions like Zn^{2+}, Fe^{2+}, and Cu^{+} have equal importance in complex cellular processes, but the development of analogous tools only began recently.[5,6]

Free or chelatable zinc is present in the mammalian forebrain where it is stored within the synaptic vesicles of glutamatergic neurons.[7] Neuronal activity releases vesicular zinc into the synaptic cleft, which modulates the activity of many synaptic targets. While synaptic zinc functions have not been elucidated fully, Zn^{2+} can bind to GABA (γ-aminobutyric acid) and NMDA (*N*-methyl-D-aspartate) receptors as well as regulate activity of many postsynaptic channels.[8] Zinc may function as a neural signaling agent in healthy individuals, but it may also be involved in many neurological diseases.[9,10] Homeostasis disruptions can produce severe consequences leading to imbalances in intracellular $[Zn^{2+}]$. Excess Zn^{2+} can accumulate within cells and lead to damage and death. We have focused on designing new Zn^{2+} photocages to explore potential signaling functions and disease pathology.[11−14]

Inspired by the Nitr family of photocages for Ca^{2+}, we developed ZinCast-1,[13] a Zn^{2+} photocage that integrates a *N*,*N*-dipicolylaniline (DPA) ligand with a light sensitive *o*-nitrobenzyl moiety. The metal ion release in $[Zn(ZinCast\text{-}1)]^{2+}$ relies on attenuation of the aniline nitrogen atom−Zn^{2+} bond strength upon light-initiated formation of the nitrosobenzophenone photoproduct $[Zn(ZinUnc\text{-}1)^{2+}]$ (Scheme 1). The resonance delocalization of the anilino lone pair onto the newly formed carbonyl group decreases the Zn^{2+} affinity and shifts the binding equilibrium toward solvated metal ion. Change in metal affinity due to photolysis can be expressed quantitatively by ΔK_d, which is a ratio of photoproduct's dissociation constant

Received: February 21, 2013
Published: July 10, 2013

   dx.doi.org/10.1021/ic400465g | *Inorg. Chem.* 2013, 52, 8483−8494

Scheme 1. Uncaging process in ZinCast-1

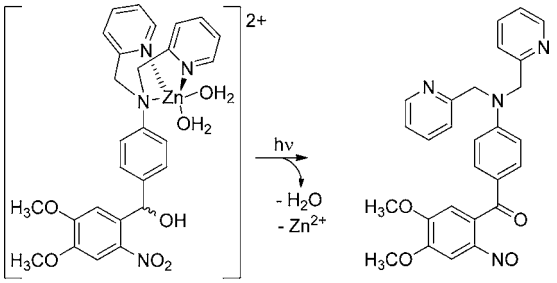

(ZinUnc K_d) to the dissociation constant of the photocage (ZinCast K_d), ΔK_d = (ZinUnc K_d)/(ZinCast K_d).

Additional complementary ZinCast photocages differ only in Zn^{2+}-receptor design, where the methylene linker between aniline nitrogen and the pyridine moiety of ZinCast-1 was extended to an ethylene on one (ZinCast-2) or both spacers (ZinCast-3).[14] While all three ZinCast photocages exhibit reduced Zn^{2+} affinity following photolysis, the most pronounced changes occur in ZinCast-3, which has the lowest Zn^{2+} affinity. In contrast, ZinCast-1 forms the highest affinity pre-photolysis Zn^{2+} complex, but a reduced ΔK_d upon uncaging. An analogous trend was observed for Cast type photocages that utilize crown ether ligands.[15,16] These results indicate that increased chelator affinity in the Zn^{2+} complexes reduces metal ion release efficiency. Complexes containing more weakly binding chelators exhibit significantly larger changes in Zn^{2+} affinity upon photolysis, but the low affinity prohibits use in biology where proteins maintain Zn^{2+} homeostasis at minimal basal levels.[17] Addressing these practical problems requires designing a photocage possessing a high affinity for Zn^{2+} that decreases drastically upon uncaging.

To maximize the Zn^{2+} offloading capability with concurrent preservation of pre-photolysis metal ion buffering capacity, we envisioned introducing a second *o*-nitrobenzyl photocaging group. Utilization of two photolabile groups in photocages has precedent in organic synthesis[18] as well as in small molecule photocages.[19] In the first Ca^{2+} photocage utilizing two photolabile groups Nitr-8, the affinity of the Ca^{2+}-selective chelator decreases 1600-fold upon uncaging; however, Nitr-8 was reported in a review that lacked extensive characterization data.[4] In the structurally related photocage Nitr-T that also contains two nitrobenzyl groups, the Ca^{2+} affinity decreases >3000-fold from the pre-photolysis Ca^{2+} K_d of 520 nM.[20] The photoproducts resulting from photolysis of Nitr-8 and Nitr-T photocages contain two metal-bound aniline nitrogen atoms with reduced electron density compared to the corresponding photocaged complex. While inclusion of a second photocaging group has been implemented for Ca^{2+}, this strategy has not

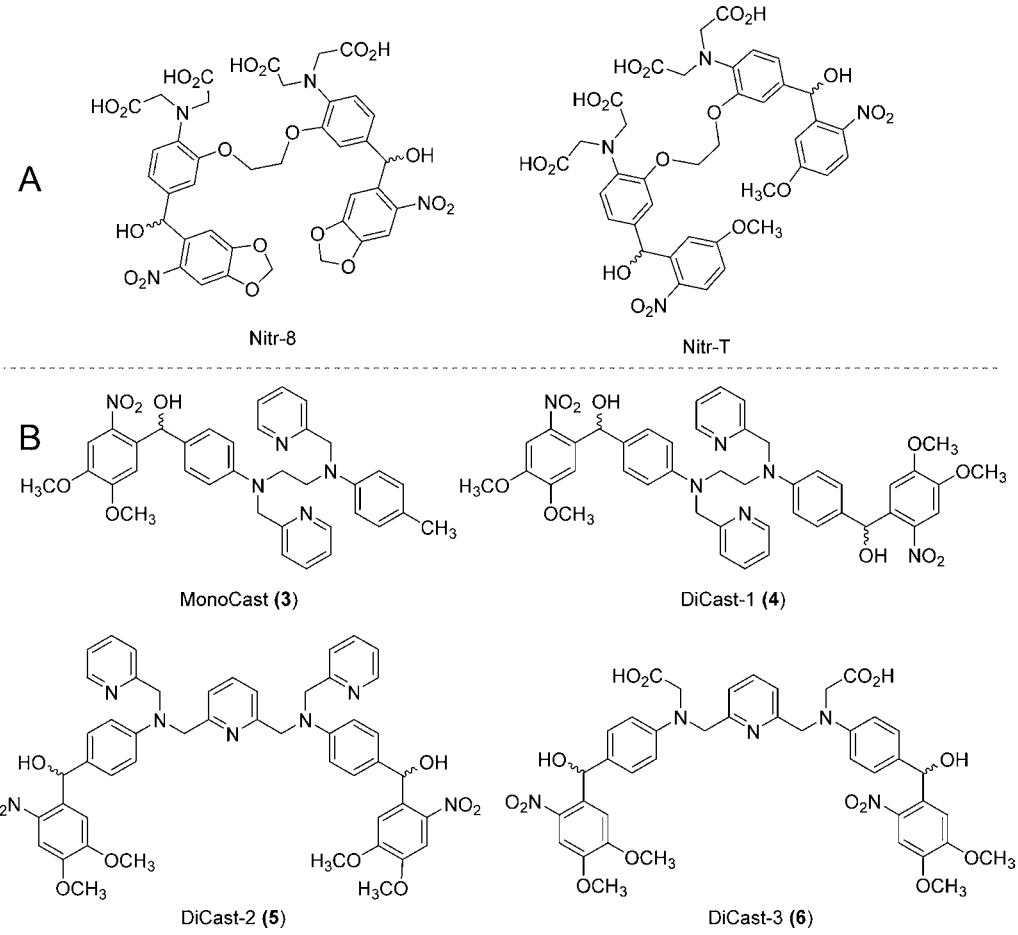

Figure 1. (A) Structures of Ca^{2+} photocages Nitr-8 and Nitr-T that utilize two nitrobenzyl groups. (B) Structures of MonoCast, DiCast-1, DiCast-2, and DiCast-3. MonoCast and DiCast-1 allow the direct comparison of the effects from using a single versus two nitrobenzyl groups. DiCast-2 and DiCast-3 are second generation DiCast photocages designed to have higher affinity for Zn^{2+}.

dx.doi.org/10.1021/ic400465g | *Inorg. Chem.* 2013, 52, 8483−8494

been explored for other metal ions with different coordination chemistry requirements.

By combining the multi-photolabile group strategy utilized in Ca^{2+} photocages with Zn^{2+}-binding properties of ZinCast-1, new photocaged chelators were envisioned with increased Zn^{2+} stability and increased ΔK_d upon uncaging. The DiCast photocage nomenclature evokes the original Cast series,[13−16,21−23] where the suffix implies release by "casting off", and adds the prefix "Di-" indicating the presence of two nitrobenzyl groups. To quantify the magnitude of ΔK_d changes induced by two photocaging groups, MonoCast-1 and DiCast-1 were designed to mimic elements of the 3-nitrogen donor-based DPA ligand of ZinCast-1 and the 4-nitrogen donor chelator EBAP (ethylene-bis-α,α'-(2-aminomethyl)pyridine). A modular synthetic strategy provided access to derivatives that could be functionalized with 1 or 2 nitrobenzyl groups. Since the receptor in MonoCast-1 and DiCast-1 contains only an additional aniline ligand when compared to ZinCast-1, only a modest increase in absolute Zn^{2+} affinity was anticipated, but the photocages would allow a direct comparison of ΔK_d trends. To increase photocage metal ion affinity, a second generation of DiCast photocages was designed with additional chelating ligands (Figure 1). Replacement of the ethylene linker in DiCast-1 chelator by a bridging pyridine leads to increase in ligand denticity and reduces ligand flexibility to further increase binding strength. DiCast-2 retains the aniline and pyridine ligands; however, carboxylates were used in DiCast-3 to enhance water solubility.

EXPERIMENTAL SECTION

General Experimental. All materials were purchased from Acros Organic or TCI America. Solvents were sparged with argon and dried in Seca Solvent Purification System. *N*,*N*′-Diphenylethane-1,2-diamine (**13**)[24−26] and 2,6-bis-(bromomethyl)pyridine (**16**)[27] was prepared as previously described. Bulk photolysis was carried out using a 1000 W lamp with λ = 300−800 nm. All chromatography and TLC were performed on silica from Silicycle or activated basic alumina from Acros Organics. ^{1}H and ^{13}C NMR spectra were recorded with a Bruker 400 MHz spectrometer and referenced to $CDCl_3$. IR spectra were recorded on a Nicolet 205 FT-IR instrument, and samples were analyzed as KBr pellets. High resolution mass spectra were obtained on a Waters Micromass Q-Tof-2 mass spectrometer at the University of Connecticut Biotechnology-Bioservices Center or a Bruker micrOTOF II at the University of Notre Dame Mass Spectrometry & Proteomics Facility operating in positive ion mode. The instrument was calibrated with Glu-fibrinopeptide B 10 pmol/μL by using a 50:50 solution of CH_3CN/H_2O with 0.1% acetic acid.

*N-Phenyl-N′-(p-tolyl)ethane-1,2-diamine (**9**).* Tris-(dibenzylideneacetone)dipalladium ($Pd_2(dba)_3$) (40 mg, 1 mol %), 2,2′-bis(diphenylphosphino)-1,1′-binaphthyl (BINAP, 82 mg, 3 mol %), NaO*t*Bu (1.27 g, 1.32 mmol), and degassed toluene (15 mL) were combined in a Schlenk tube. *N*-Phenylethylenediamine (**7**, 636 μL, 4.86 mmol) and *p*-bromotoluene (**8**, 544 μL, 4.42 mmol) were successively added, and the reaction mixture was stirred at 80 °C. After 24 h, the reaction mixture was cooled, diluted with H_2O (30 mL), extracted with EtOAc (3 × 30 mL), and dried over $MgSO_4$ and the solvent was removed. Flash chromatography on silica (1:4 EtOAc/hexanes) yielded **9** as a yellow solid (0.481 g, 48.1%). Mp: 44−45 °C. ^{1}H NMR (400 MHz, $CDCl_3$): δ 7.18 (t, J = 8.0 Hz, 2 H), 7.00 (d, J = 8.0 Hz, 2 H), 6.72 (t, J = 8.0 Hz, 1 H), 6.64 (d, J = 8.0 Hz, 2 H), 6.57 (d, J = 8.0 Hz, 2 H), 3.78 (s, 2 H), 3.37 (s, 4 H), 2.24 (s, 3 H). ^{13}C NMR (100 MHz, $CDCl_3$): δ 148.31, 145.99, 130.04, 129.54, 127.33, 117.99, 113.46, 113.24, 43.93, 43.61, 20.59. IR (KBr pellet, cm^{-1}): 3418, 3408, 1601, 1525, 1459, 1341, 1294, 1263, 1209, 1178, 1135, 1090. HRMS (+ESI): calcd for MH$^+$, 227.1548; found, 227.1552.

*N-Phenyl-N,N′-bis(pyridin-2-ylmethyl)-N′-(p-tolyl)ethane-1,2-diamine (**10**).* To a solution of **9** (0.464 g, 2.05 mmol) in CH_3CN (30 mL) were added 2-(bromomethyl)pyridine hydrobromide (1.55 g, 6.15 mmol), potassium hydrogen phosphate (K_2HPO_4) (2.14 g, 12.3 mmol), and KI (0.34 g, 2.05 mmol). After the reaction mixture was refluxed overnight, the solvent was removed, water (30 mL) was added, and pH was adjusted to approximately 9. The crude product was extracted with EtOAc (3 × 50 mL) and dried over $MgSO_4$. Flash chromatography on basic alumina (2:3 EtOAc/hexanes) yielded **10** as a yellow solid (0.653 g, 75.4%). Mp: 90−91 °C. ^{1}H NMR (400 MHz, $CDCl_3$): δ 8.55 (s, 2 H), 7.52 (t, J = 4.0 Hz, 2 H), 7.17−7.11 (m, 6 H), 6.97 (d, J = 8.0 Hz, 2 H), 6.68 (m, 3 H), 6.60 (d, J = 8.0 Hz, 2 H), 4.64 (d, J = 8.0 Hz, 4 H), 3.73 (s, 4 H), 2.20 (s, 3 H). ^{13}C NMR (100 MHz, $CDCl_3$): δ 159.47, 159.26, 149.85, 149.79, 147.96, 145.82, 136.90, 130.19, 129.65, 126.40, 122.18, 122.15, 121.15, 121.04, 117.07, 112.39, 57.54, 57.28, 49.08, 48.98, 20.38. IR (KBr pellet, cm^{-1}): 1616, 1590, 1570, 1520, 1505, 1475, 1459, 1445, 1431, 1386, 1344, 1211, 1167, 994, 941. HRMS (+ESI): calcd for MH$^+$, 409.2392; found, 409.2389.

*(4,5-Dimethoxy-2-nitrophenyl)(4-((pyridin-2-ylmethyl)(2-((pyridin-2-ylmethyl)(p-tolyl)amino)ethyl)amino)phenyl)methanol (MonoCast, **3**).* Trimethylsilyl trifluoromethanesulfonate (TMSOTf) (0.74 mL, 4.08 mmol) and 2,6-lutidine (0.63 mL, 5.44 mmol) were added successively to a mixture of **10** (0.575 g, 1.36 mmol) and 6-nitroveratraldehyde (**11**, 0.374 g, 1.76 mmol) in CH_2Cl_2 (40 mL). The resulting solution was stirred for 6 h, and then tetrabutylammonium fluoride (TBAF) in THF (1 M, 4.1 mL, 4.08 mmol) was added to the reaction mixture. After 1 h, the solvent was removed under reduced pressure. Flash chromatography on basic alumina (1:4 hexanes/EtOAc) afforded **3** as a yellow solid (0.632 g, 75.0%). Mp: 136−137 °C. ^{1}H NMR (400 MHz, $CDCl_3$): δ 8.52 (s, 2 H), 7.58 (s, 1 H), 7.51 (t, J = 4.0 Hz, 2 H), 7.39 (s, 1 H), 7.11−7.05 (m, 6 H), 6.95 (d, J = 8.0 Hz, 2 H), 6.57 (d, J = 8.0 Hz, 4 H), 6.45 (d, J = 4.0 Hz, 1 H), 4.59 (d, J = 4.0 Hz, 4 H), 3.94 (s, 3 H), 3.91 (s, 3 H), 3.69 (s, 4 H), 2.86 (d, J = 4.0 Hz, 1 H), 2.19 (s, 3 H). ^{13}C NMR (100 MHz, $CDCl_3$): δ 159.33, 158.91, 153.55, 149.82, 149.72, 147.87, 147.63, 145.67, 140.10, 136.96, 135.02, 130.52, 130.19, 128.68, 126.45, 122.25, 122.19, 121.15, 120.99, 112.67, 112.12, 110.31, 108.30, 71.45, 57.46, 57.13, 56.63, 56.55, 48.97, 20.37. IR (KBr pellet, cm^{-1}): 3105, 1596, 1570, 1520, 1507, 1470, 1433, 1360, 1335, 1276, 1248, 1235, 1211, 1159, 1066, 1027. HRMS (+ESI): calcd for MH$^+$, 620.2828; found, 620.2819.

*(4,5-Dimethoxy-2-nitrosophenyl)(4-((pyridin-2-ylmethyl)(2-((pyridin-2-ylmethyl)(p-tolyl)amino)ethyl)amino)phenyl)methanone (MonoUnc, **12**).* Photolysis of **3** (57 mg, 0.92 mmol) in 3 mL of CH_3CN for 8 h followed by chromatography on basic alumina (1:1 EtOAc/hexanes) yielded MonoUnc as an orange oil (26 mg, 47%). ^{1}H NMR (400 MHz, $CDCl_3$): δ 8.53 (t, J = 8.0 Hz, 2 H), 7.66 (d, J = 8.0 Hz, 2 H), 7.53 (q, J = 4.0 Hz, 2 H), 7.13−7.08 (m, 4 H), 7.02−6.96 (m, 3 H), 6.59 (t, J = 8.0 Hz, 4 H), 6.30 (s, 1 H), 4.66 (s, 2 H), 4.58 (s, 2 H), 4.01 (s, 3 H), 3.88 (s, 3 H), 3.79 (d, J = 4.0 Hz, 2 H), 3.72 (d, J = 4.0 Hz, 2 H), 2.20 (s, 3 H). ^{13}C NMR (100 MHz, $CDCl_3$): δ 193.99, 160.05, 159.05, 157.52, 156.01, 152.23, 150.16, 150.09, 149.78, 145.60, 140.14, 137.12, 136.96, 132.90, 130.28, 127.73, 126.93, 122.57, 122.31, 121.33, 120.81, 112.97, 111.19, 109.82, 91.90, 57.67, 77.55, 77.23, 76.92, 57.67, 57.00, 56.91, 56.42, 49.08, 48.80, 20.39. IR (KBr, cm^{-1}): 2926, 1611, 1590, 1570, 1463, 1434, 1328, 1268, 1207, 1179, 1062, 908, 796. HRMS (+ESI): calcd for MH$^+$, 602.2767; found, 602.2771.

*N,N′-Diphenyl-N,N′-bis(pyridin-2-ylmethyl)ethane-1,2-diamine (**14**).* Synthesis of **14** followed the same procedure as synthesis of **10** using compound **13** (1.01g, 4.76 mmol), 2-(bromomethyl)pyridine hydrobromide (3.00g, 11.9 mmol), potassium hydrogen phosphate (K_2HPO_4) (4.14 g, 23.8 mmol), and KI (0.789 g, 4.76 mmol). Flash chromotography on basic alumina using a solvent gradient (1:2 to 3:2 EtOAc/hexanes) afforded **14** as a white crystalline solid (1.26 g, 64.9%). Mp: 141−142 °C. ^{1}H NMR (400 MHz, $CDCl_3$): δ 8.56 (d, J = 8.0 Hz, 2 H), 7.54 (t, J = 8.0 Hz, 2 H), 7.18−7.12 (m, 8 H), 6.70−6.67 (m, 6 H), 4.66 (s, 4 H), 3.76 (s, 4 H). ^{13}C NMR (100 MHz, $CDCl_3$): δ 159.20, 149.87, 147.95, 16.93, 129.67, 122.21, 121.07, 117.16, 112.43, 57.29, 48.90. IR (KBr pellet, cm^{-1}): 1597, 1588, 1571, 1506, 1469, 1443, 1432, 1394, 1351, 1341, 1215, 1170, 991, 941, 750. HRMS (+ESI): calcd for MH$^+$, 395.2236; found, 395.2221.

dx.doi.org/10.1021/ic400465g | *Inorg. Chem.* 2013, 52, 8483−8494

*((Ethane-1,2-diylbis((pyridin-2-ylmethyl)azanediyl))bis(4,1-phenylene))bis((4,5-dimethoxy-2-nitrophenyl)methanol) (DiCast-1, **4**).* Synthesis of DiCast-1 followed the same procedure as synthesis of MonoCast using **14** (0.310 g, 0.759 mmol), **11** (0.353 g, 1.51 mmol), 2,6-lutidine (0.62 mL, 5.31 mmol), TMSOTf (0.69 mL, 3.80 mmol), and 1 M TBAF (4.54 mmol). Flash chromatography on basic alumina (1:99 MeOH/EtOAc) yielded DiCast-1 as an orange solid (0.398 g, 64.2%). Mp: 106−108 °C. ^{1}H NMR (400 MHz, $CDCl_3$): δ 8.50 (d, J = 4.0 Hz, 2 H), 7.57 (s, 2 H), 7.50 (t, J = 8.0 Hz, 2 H), 7.42 (s, 2 H), 7.11−7.03 (m, 8 H), 6.54 (d, J = 8.0 Hz, 4 H), 6.44 (d, J = 4.0 Hz, 2 H), 4.48 (s, 4 H), 3.94 (s, 6 H), 3.90 (s, 6 H), 3.65 (s, 4 H), 3.16 (d, J = 4.0 Hz, 2 H). ^{13}C NMR (100 MHz, $CDCl_3$): δ 158.80, 153.58, 149.76, 147.87, 147.50, 140.08, 137.09, 135.05, 130.90, 128.75, 122.33, 121.02, 112.23, 110.28, 108.34, 71.39, 57.11, 56.64, 56.55, 48.94. IR (KBr pellet, cm^{-1}): 3510, 1611, 1571, 1517, 1462, 1437, 1392, 1330, 1271, 1215, 1179, 1063, 911. HRMS (+ESI): calcd for MH$^+$, 817.3197; found, 817.3338.

*((Ethane-1,2-diylbis((pyridin-2-ylmethyl)azanediyl))bis(4,1-phenylene))bis((4,5-dimethoxy-2-nitrosophenyl)methanone) (DiUnc-1, **15**).* Photolysis of **4** (57 mg, 0.070 mmol) for 16 h followed by flash chromatography on basic alumina (EtOAc) afforded DiUnc-1 as a yellow oil (12 mg, 22%). ^{1}H NMR (400 MHz, $CDCl_3$): δ 8.52 (d, J = 4.0 Hz, 2 H), 7.67 (d, J = 8.0 Hz, 4 H), 7.56 (t, J = 8.0 Hz, 2 H), 7.14 (t, J = 8.0 Hz, 2 H), 7.08 (s, 2 H), 7.03 (d, J = 8.0 Hz, 2 H), 6.60 (d, J = 8.0 Hz, 4 H), 6.31 (s, 2 H), 4.65 (s, 4 H), 4.01 (s, 6 H), 3.88 (s, 6 H), 3.84 (s, 4 H). ^{13}C NMR (100 MHz, $CDCl_3$): δ 194.10, 160.05, 157.18, 156.08, 151.97, 150.24, 150.17, 139.94, 137.23, 132.95, 128.14, 122.78, 121.02, 111.45, 111.21, 109.81, 107.07, 91.97, 57.03, 56.88, 56.43, 48.84. IR (KBr): 1608, 1587, 1514, 1452, 1381, 1327, 1267, 1217, 1180, 1061, 1023, 1003, 819, 795, 758 cm^{-1}. (+ESI): calcd for MH$^+$, 781.2986; found, 781.3120.

*N,N′-(Pyridine-2,6-diylbis(methylene))dianiline (**17**).* Synthesis of **17** followed the same procedure as synthesis of **10** using **16** (2.16 g, 8.15 mmol), aniline (2.23 mL, 24.4 mmol), K_2HPO_4 (5.68 g, 32.6 mmol), and KI (1.35 g, 8.15 mmol). The product was extracted with CH_2Cl_2 instead of EtOAc. Flash chromatography on silica using a solvent gradient (1:4 to 2:3 EtOAc/hexanes) yielded **17** as a yellow oil (1.08 g, 45.8%). ^{1}H NMR (400 MHz, $CDCl_3$): δ 7.58 (t, J = 8.0 Hz, 1 H), 7.22−7.16 (m, 6 H), 6.74 (t, J = 8.0 Hz, 2 H), 6.68 (d, J = 8.0 Hz, 4 H), 4.73 (s, 2 H), 4.47 (s, 4 H). ^{13}C NMR (100 MHz, $CDCl_3$): δ 158.28, 148.11, 137.42, 129.46, 120.06, 117.83, 113.27, 49.45. IR (KBr, cm^{-1}): 3414, 3050, 1603, 1575, 1506, 1455, 1429, 1317, 1260, 1179, 749, 692. HRMS (+ESI): calcd for MH$^+$, 290.1657; found, 290.1615.

*N,N′-(Pyridine-2,6-diylbis(methylene))bis(N-(pyridin-2-ylmethyl)-aniline) (**18**).* 2-Pyridinecarboxaldehyde (1.05 mL, 18.4 mmol) and **17** (1.07 g, 3.69 mmol) were combined in CH_2Cl_2 (40 mL) with sodium triacetoxyborohydride (2.35 g, 18.4 mmol). After 24 h, the reaction mixture was washed with saturated $NaHCO_3$ (40 mL) and saturated NaCl (40 mL). The solvent was removed and recrystallization from EtOAc yielded **18** as a white solid (0.883 g, 50.7%). Mp: 181−182 °C. ^{1}H NMR (400 MHz, $CDCl_3$): δ 8.58 (d, J = 4.0 Hz, 2 H), 7.61−7.51 (m, 3 H), 7.25 (d, J = 8.0 Hz, 2 H), 7.17−7.11 (m, 8 H), 6.72−6.68 (m, 6 H), 4.81 (s, 4 H), 4.78 (s, 4 H). ^{13}C NMR (100 MHz, $CDCl_3$): δ 159.12, 159.07, 149.91, 148.49, 137.80, 137.00, 129.51, 122.21, 121.01, 119.33, 117.40, 112.69, 57.47, 57.45. IR (KBr pellet, cm^{-1}): 1600, 1593, 1570, 1506, 1461, 1388, 1348, 1245, 1225, 1181, 986, 946, 780, 756, 744. HRMS (+ESI): calcd for MH$^+$, 472.2501; found, 472.2474.

*(((Pyridine-2,6-diylbis(methylene))bis((pyridin-2-ylmethyl)-azanediyl))bis(4,1-phenylene))bis((4,5-dimethoxy-2-nitrophenyl)-methanol) (DiCast-2, **5**).* A solution of **18** (0.362 g, 0.767 mmol) and **11** (0.356 g, 1.53 mmol) in CH_2Cl_2 was cooled to 0 °C, and 2,6-lutidine (0.62 mL, 5.36 mmol) and TMSOTf (0.695 mL, 3.83 mmol) were added. The reaction mixture was stirred overnight, and TBAF (1 M, 4.6 mL, 4.6 mmol) was added. After 1 h, the solvent was removed under reduced pressure. Recrystallization from CH_3OH yielded DiCast-2 as a yellow crystalline solid (0.205 g, 30.0%). Mp: 134−136 °C. ^{1}H NMR (400 MHz, $CDCl_3$): δ 8.53 (d, J = 4.0 Hz, 2 H), 7.79 (d, J = 4.0 Hz, 2 H), 7.64−7.57 (m, 5 H), 7.31 (d, J = 8.0 Hz, 2 H), 7.16−7.19 (m, 6 H), 7.04 (t, J = 8.0 Hz, 2 H), 6.86 (s, 2 H), 6.53 (d, J = 4.0 Hz, 2 H), 6.20 (d, J = 8.0 Hz, 2 H), 4.80−4.53 (m, 4 H), 3.98 (s, 3 H), 3.96 (s, 3 H), 3.89 (s, 6 H), 3.54−3.49 (m, 4 H). ^{13}C NMR (100 MHz, $CDCl_3$): δ 160.41, 160.31, 155.88, 153.57, 149.04, 148.96, 147.42, 139.75, 137.91, 137.91, 137.28, 136.57, 131.99, 131.90, 128.62, 122.15, 120.77, 119.80, 112.94, 109.82, 108.34, 71.22, 57.47, 56.67, 56.62, 56.54, 55.10. IR (KBr pellet, cm^{-1}): 3280, 1612, 1576, 1520, 1436, 1384, 132, 1270, 1217, 1179, 1062, 815, 796, 749. HRMS (+ESI): calcd for MH$^+$, 894.3463; found, 894.2460.

*(((Pyridine-2,6-diylbis(methylene))bis((pyridin-2-ylmethyl)-azanediyl))bis(4,1-phenylene))bis((4,5-dimethoxy-2-nitrosophenyl)-methanone) (DiUnc-2, **19**).* Photolysis of **5** (54 mg, 0.060 mmol) for 16 h followed by chromatography on silica (1:99 CH_3OH−CH_2Cl_2) lead to isolation of DiUnc-2 as a yellow oil (10 mg, 19%). ^{1}H NMR (400 MHz, $CDCl_3$): δ 8.54 (d, J = 4.0 Hz, 2 H), 7.65 (d, J = 12.0 Hz, 4 H), 7.60−7.55 (m, 3 H), 7.17−7.04 (m, 8 H), 6.61 (d, J = 8.0 Hz, 4 H), 6.28 (s, 2 H), 4.79 (s, 4 H), 3.99 (s, 3 H), 3.86 (s, 3 H), 3.62−3.57 (m, 10 H). ^{13}C NMR (100 MHz, $CDCl_3$): δ 194.12, 160.07, 157.79, 157. 54, 156.08, 152.86, 150.20, 150.14, 138.12, 137.20, 132.74, 128.21, 122.65, 120.96, 119.76, 111.77, 109.83, 91.88, 60.63, 57.32, 57.04, 56.44. HRMS (+ESI): calcd for MH$^+$, 858.3251; found, 858.4223.

*Diethyl 2,2′-((Pyridine-2,6-diylbis(methylene))bis-(phenylazanediyl))diacetate (**20**).* Synthesis of **20** followed the same procedure as synthesis of **10** using **17** (0.930 g, 3.21 mmol), ethyl bromoacetate (0.85 mL, 23.3 mmol), K_2HPO_4 (3.36 g, 19.3 mmol), and KI (0.533 g, 3.21 mmol). The product was extracted with CH_2Cl_2 instead of EtOAc. Flash chromotography on silica with a solvent gradient (1:4 to 2:3 EtOAc/Hex) yielded **20** as a yellow oil (1.15 g, 77.4%). ^{1}H NMR (400 MHz, $CDCl_3$): δ 7.52 (t, J = 8.0 Hz, 1 H), 7.24−7.17 (m, 6 H), 6.75 (t, J = 8.0 Hz, 2 H), 6.66 (d, J = 8.0 Hz, 4 H), 4.73 (s, 4 H), 4.24−4.17 (m, 8 H), 1.26 (t, J = 8.0 Hz, 6 H). ^{13}C NMR (100 MHz, $CDCl_3$): δ 171.22, 159.02, 148.29, 137.79, 129.45, 119.52, 117.93, 112.65, 61.30, 58.43, 53.85, 14.45. IR (KBr pellet, cm^{-1}): 1744, 1598, 1575, 1504, 1447, 1383, 1346, 1260, 1177, 1023, 990, 958, 746, 690. HRMS (+ESI): calcd for MH$^+$, 462.2393; found, 462.2395.

*Diethyl 2,2′-((Pyridine-2,6-diylbis(methylene))bis((4-((4,5-dimethoxy-2-nitrophenyl)(hydroxy)methyl)phenyl)azanediyl))diacetate (**21**).* A solution of **20** (0.139 g, 0.301 mmol) and **11** (0.127 g, 0.602 mmol) in 10 mL of CH_2Cl_2 was cooled to −10 °C, and 2,6-lutidine (868 μL, 0.602 mmol) and TMSOTf (135 μL, 0.602 mmol) were added over 1 h. The resulting solution was stirred for 6 h, and then TBAF in THF (1 M, 1.8 mL, 1.8 mmol) was added to the reaction mixture. After 1 h the solvent was removed under reduced pressure. Recrystallization from CH_3OH yielded **21** as a yellow crystalline solid (0.130 g, 48.9%). Mp: 79−81 °C. ^{1}H NMR (400 MHz, $CDCl_3$): δ 7.58 (s, 2 H), 7.50 (t, J = 8.0 Hz, 1 H), 7.39 (s, 2 H), 7.16−7.09 (m, 6 H), 6.51 (d, J = 8.0 Hz, 4 H), 6.44 (s, 2 H), 4.65 (s, 4 H), 4.17 (q, J = 8.0 Hz, 4 H), 4.03 (d, J = 8.0 Hz, 4 H), 3.95 (s, 6 H), 3.91 (s, 6 H), 2.76 (s, 2 H), 1.23 (t, J = 8.0 Hz, 6 H). ^{13}C NMR (100 MHz, $CDCl_3$): δ 171.22, 158.55, 153.54, 148.05, 147.87, 140.11, 137.81, 134.91, 131.39, 128.45, 119.65, 112.53, 110.31, 108.30, 71.48, 61.41, 58.07, 56.63, 56.56, 53.90, 14.44. IR (KBr pellet, cm^{-1}): 3513, 1731, 1611, 1575, 1513, 1461, 1385, 1267, 1205, 1178, 1060, 1022, 984, 960. HRMS (+ESI): calcd for MH$^+$, 884.3354; found, 884.3304.

*2,2′-((Pyridine-2,6-diylbis(methylene))bis((4-((4,5-dimethoxy-2-nitrophenyl)(hydroxy)methyl)phenyl)azanediyl))diacetic Acid (DiCast-3, **6**).* To a solution of **21** (0.080 g, 0.090 mmol) in THF (1 mL) were added 1 M KOH (0.27 mL, 0.27 mmol) and 1 mL of H_2O. The resultant solution was stirred overnight at room temperature, 10 mL of water was added, and product was precipitated by a dropwise addition of acetic acid until no more solid formed. The resulting yellow solid was collected by filtration and dried under nitrogen (0.026 g, 65%). Mp: 169−171 °C. ^{1}H NMR (400 MHz, DMSO) 7.55−7.47 (m, 5 H), 7.27 (d, J = 8 Hz, 2 H), 6.87 (d, J = 8.0 Hz, 4 H), 6.35 (d, J = 8.0 Hz, 4 H), 4.52 (s, 4 H), 3.92 (s, 6 H), 3.85 (s, 6 H), 3.53 (s, 4 H). ^{13}C NMR (100 MHz, DMSO): δ 171.78, 159.71, 152.84, 148.46, 147.00, 139.31, 135.84, 129.72, 127.56, 118.85, 111.04, 109.94, 107.72, 79.16, 69.33, 58.01, 56.70, 56.05, 55.99. IR (KBr pellet, cm^{-1}): 3382,

dx.doi.org/10.1021/ic400465g | Inorg. Chem. 2013, 52, 8483−8494

1575, 1513, 1452, 1382, 1326, 1268, 1215, 1179, 1060, 1024, 983, 817, 795, 746. HRMS (+ESI): calcd for MH^+, 828.2728; found, 828.2774.

*2,2′-((Pyridine-2,6-diylbis(methylene))bis(phenylazanediyl))-diacetic Acid (**23**).* Deprotection of **20** (0.59 g, 1.3 mmol) followed the same procedure as deprotection of **6** using 1 M KOH (5.1 mL, 5.1 mmol). After precipitation and drying, **23** was obtained as a white solid (0.41 g, 80%). Mp: 199−201 °C. ^{1}H NMR (400 MHz, DMSO): δ 7.77 (t, J = 8.0 Hz, 1 H), 7.35 (d, J = 8 Hz, 2 H), 7.09 (t, J = 8.0 Hz, 4 H), 6.63 (t, J = 8 Hz, 2 H), 6.48 (d, J = 8 Hz, 4 H), 4.70 (s, 4 H), 4.28 (s, 4 H). ^{13}C NMR (100 MHz, DMSO): δ 172.60, 158.59, 147.38, 138.62, 129.01, 119.99, 116.70, 111.80, 56.91, 54.00. IR (KBr pellet, cm^{-1}): 1570, 1504, 1450, 1391, 1349, 1322, 1295, 1229, 1179, 988, 958, 898, 784, 770, 745, 690. HRMS (+ESI): calcd for MH^+, 406.1767; found, 406.1770.

[Zn(18)][Zn(NO$_3$)$_4$]. The ligand **18** (20.0 mg, 0.042 mmol) was combined with $Zn(NO_3)_2{\cdot}4H_2O$ (22.0 mg, 0.084 mmol) in 1:1 CH_3CN/CH_2Cl_2 and refluxed for 2 h. Colorless blocks where obtained by vapor diffusion with diethyl ether. IR (KBr pellet, cm^{-1}): 3060, 2388, 1614, 1587, 1495, 1467, 1440, 1380, 1353, 1321, 1286, 1259, 1186, 1161, 1126, 1100, 1060, 1032, 1015, 982, 934, 898, 838, 812. HRMS (+ESI): calcd for [Zn(**18**)]H^+, 536.1793; found, 536.1787.

[Zn$_3$K(23)$_2$(H$_2$O)Cl$_3$]. The ligand **23** was washed with a concentrated solution of KOH in EtOH and dried. Stock solutions of **23** (135 μL, 0.0839 M, 0.011 mmol) and $ZnCl_2$ (75 μL, 0.182 M, 0.014 mmol) in CH_3CN were combined with pyridine (3.5 μL, 0.044 mmol). The solution was diluted with 1 mL of CH_3CN and placed in a diffusion chamber with hexanes to provide colorless needles. IR (KBr pellet, cm^{-1}): 3586, 3066, 2890, 2323, 2166, 2036, 1646, 1625, 1599, 1576, 1497, 1467, 1441, 1410, 1385, 1327, 1289, 1261, 1243, 1207, 1162, 1134, 1096, 1026, 932, 888, 844. HRMS (+ESI): calcd for MH^+, 1160.9825; found, 1160.9820.

Binding Constants. Absorption spectra were recorded on a Cary 50 UV−visible spectrophotometer run under Varian's Cary WinUV software. All spectra were acquired at 25 °C in quartz cuvettes with path length of 1 cm and cell volume of 3.0 mL. Stock solutions of photocages were prepared at mM concentrations in DMSO and diluted to prepare 25 μM solutions in the solvent of choice. All metal binding constants were determined by previously described procedures. Aqueous stock solutions of the metal perchlorate salts of Cu^{2+}, Zn^{2+}, and Cd^{2+} were prepared in mM concentrations. A 25 μM solution of the ligand was prepared in 3000 μL of the solvent and titrated in triplicate with each of the metal salt stock solutions. Absorption spectra were corrected for dilution, and the conditional dissociation constants (K_d) were calculated using XLfit.[28]

Collection and Reduction of X-ray Data. Structural analysis was carried out in the X-ray Crystallographic Facility at Worcester Polytechnic Institute. Crystals were covered in PARATONE oil on 100 μm MiTeGen polyimide micromounts or glued on the tip of a glass fiber and were mounted on a Bruker-AXS APEX CCD diffractometer equipped with an LT-II low temperature device. Diffraction data were collected at room temperature or at 100(2) K using graphite monochromated Mo Kα radiation (λ = 0.71073 Å) using the omega scan technique. Empirical absorption corrections were applied using the SADABS program.[29] The unit cells and space groups were determined using the SAINT+ program.[29] The structures were solved by direct methods and refined by full matrix least-squares using the SHELXTL program.[29] Refinement was based on F^2 using all reflections. All non-hydrogen atoms were refined anisotropically. Hydrogen atoms on carbon atoms were all located in the difference maps and subsequently placed at idealized positions and given isotropic U values 1.2 times that of the carbon atom to which they were bonded. Hydrogen atoms bonded to oxygen atoms were located and refined with isotropic thermal parameters. Mercury 1.4.2 software was used to examine the molecular structure.[30] Relevant crystallographic information is summarized in Table 1, selected bond distances and angles are provided in Tables 2 and 3, and the 50% thermal ellipsoid plots are shown in Figures 2 and 3.

Table 1. Crystallographic Parameters for DiCast Model Complexes

	[Zn(**18**)][Zn(NO$_3$)$_4$]	[Zn$_3$K(**23**)$_2$(H$_2$O)Cl$_3$]
formula	$C_{31}H_{29}N_5Zn{\cdot}N_4O_{12}Zn$	$C_{46}H_{44}Cl_3KN_6O_9Zn_3$
formula wt	850.41	1166.43
crystal size	0.20 × 0.25 × 0.40	0.06 × 0.20 × 0.40
space group	monoclinic, $P2_1/c$	monoclinic, $P2_1/c$
a, Å	10.4293(3)	22.191(3)
b, Å	15.1047(3)	16.5760(19)
c, Å	22.6113(6)	12.8734(16)
α, deg		
β, deg	102.094(1)	94.590(4)
γ, deg		
V, Å^3	3482.93(15)	4720.1(10)
Z	4	4
ρ_{calcd} (g cm^{-3})	1.622	1.641
abs coeff (cm^{-1})	1.45	1.83
temp, K	100	296
total no. of data	20511	37638
no. of unique data	6133	8294
obsd data[a]	4869	7234
R, %[b]	0.067	0.047
wR_2, %[c]	0.171	0.115
no. of params	487	621
max/min peaks, e/Å	0.56/−0.43	0.64/−0.52

[a]Observation criterion: $I > 2\sigma(1)$. [b]$R = \sum||F_o| - |F_c||/\sum|F_o|$. [c]$wR_2 = [\sum(w(F_o^2 - F_c^2)^2)/\sum w(F_o^2)^2]^{1/2}$.

Table 2. Selected Interatomic Distances (Å) and Angles (deg) for [Zn(18)][Zn(NO$_3$)$_4$]

bond lengths		bond angles	
Zn1−N1	2.286(5)	N1−Zn1−N2	157.7(2)
Zn1−N2	2.271(5)	N1−Zn1−N3	113.8(2)
Zn1−N3	2.006(5)	N1−Zn1−N4	79.0(2)
Zn1−N4	2.002(4)	N1−Zn1−N5	80.6(2)
Zn1−N5	2.018(4)	N2−Zn1−N3	81.6(2)
		N2−Zn1−N4	78.7(2)
		N2−Zn1−N5	112.2(2)
		N3−Zn1−N4	128.9(2)
		N3−Zn1−N5	104.5(2)
		N4−Zn1−N5	126.6(2)

[a]Numbers in parentheses are estimated standard deviations in the last digit(s). Atom labels are provided in Figure 2.

RESULTS AND DISCUSSION

Synthesis. The first generation DiCast compounds borrow design elements of the DPA ligand in ZinCast-1, which exhibited the highest stability for Zn^{2+} in the monofunctional nitrobenzhydrol photocages.[13] The similarity between these DiCast compounds and ZinCast-1 also allows for better comparison of metal binding and releasing properties resulting from the use of multiple rather than a single nitrobenzyl group. Dialkylation of *N,N*-diphenylethylenediamine with picolylbromide hydrobromide in the presence of potassium hydrogen phosphate and potassium iodide yields the four-nitrogen donor receptor for DiCast-1 (Scheme 2). The DiCast-1 receptor retains the structural features 5−5 chelate rings formed by ZinCast-1 when considering the second aniline nitrogen atom as a surrogate for one pyridine donor of DPA. The DiCast-1 receptor adds an additional pyridine ring that forms another 5-membered chelate ring when bound to the guest metal ion like

dx.doi.org/10.1021/ic400465g | Inorg. Chem. 2013, 52, 8483−8494

Table 3. Selected Interatomic Distances (Å) and Angles (deg) for $[Zn_3K(23)_2(H_2O)Cl_3]$

bond lengths		bond angles	
Zn1−N1	2.373(3)	N1−Zn1−N2	76.1(1)
Zn1−N2	2.085(4)	N1−Zn1−O2	159.1(1)
Zn1−O2	2.100(3)	N1−Zn1−O3	75.9(1)
Zn1−O3	2.000(3)	N1−Zn1−O5	91.4(1)
Zn1−O5	2.007(3)	N2−Zn1−O2	103.9(1)
		N2−Zn1−O3	116.6(1)
		N2−Zn1−O5	130.1(1)
		O2−Zn1−O3	85.9(1)
		O2−Zn1−O5	103.6(1)
		O3−Zn1−O5	106.2(1)
Zn2−N4	2.503(3)	N4−Zn2−N5	74.1(1)
Zn2−N5	2.065(4)	N4−Zn2−N6	130.4(1)
Zn2−N6	2.444(4)	N4−Zn2−O6	72.1(1)
Zn2−O6	2.089(3)	N4−Zn2−O7	154.6(1)
Zn2−O7	2.092(3)	N4−Zn2−Cl2	89.91(9)
Zn2−Cl2	2.264(1)	N5−Zn2−N6	73.7(1)
		N5−Zn2−O6	96.3(1)
		N5−Zn2−O7	108.8(1)
		N5−Zn2−Cl2	148.6(1)
		N6−Zn2−O6	147.9(1)
		N6−Zn2−O7	72.7(1)
		N6−Zn2−Cl2	98.64(9)
		O6−Zn2−O7	82.5(1)
		O6−Zn2−Cl2	104.48(9)
		O7−Zn2−Cl2	97.26(8)

[a]Numbers in parentheses are estimated standard deviations in the last digit(s). Atom labels are provided in Figure 3.

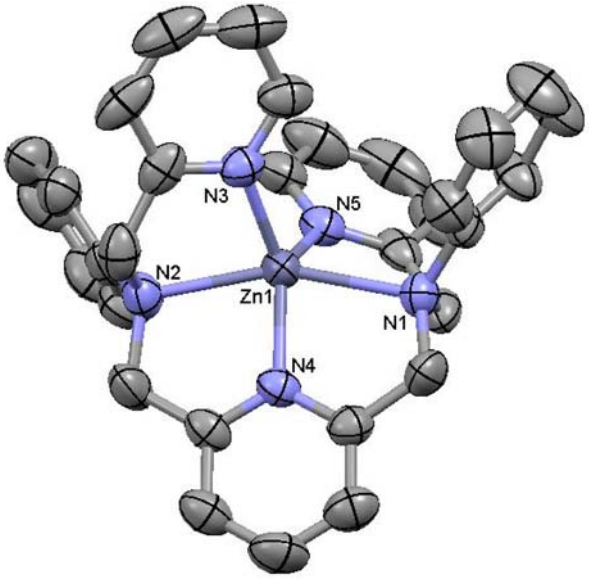

Figure 2. Perspective view of DiCast-2 model complex [Zn(**18**)][Zn-$(NO_3)_4$] showing 50% thermal ellipsoids and selected atom labels. Hydrogen atoms and $[Zn(NO_3)_4]^{2-}$ are omitted for clarity.

the aliphatic chelator EBAP. Using the TMSOTf methodology, which was originally developed for Ca^{2+} photocages and used extensively to prepare related compounds,[31] the receptor **14** was coupled to **11** (Scheme 2). Deprotection of the crude TMS ether product with TBAF affords DiCast-1 in 41% overall yield.

To provide a direct comparison between photocages that possess the same receptor but contain either a single or multiple nitrobenzyl groups, installing a methyl group onto one of the positions *para* to an aniline group in **13** was envisioned. A methyl group would block the electrophilic substitution reaction and afford a photocage with a solitary nitrobenzyl group. Coupling *N*-phenylethylenediamine and *p*-bromotoluene with Pd provides **9**, and subsequent alkylation with picolylbromide hydrobromide yields the receptor **10**. An identical TMSOTf promoted coupling reaction used to prepare DiCast-1 affords MonoCast in an overall 27% yield.

Neither MonoCast nor DiCast-1 was predicted to exhibit an exceptionally high affinity for Zn^{2+}. While adding another metal binding ligand may increase the Zn^{2+} affinity by enhancing the chelate effect, preorganized binding sites often enhance metal ion complexation.[32] A difunctional pyridine group was envisioned to act as an ideal ligand scaffold to bring together two DPA-like ligands into a symmetric receptor designed to encapsulate a single Zn^{2+} ion. Reacting **16** with excess aniline forms the backbone of the second generation DiCast photocages (Scheme 3). Excess aniline prevents overalkylation to unwanted higher order products. The common intermediate **17** provides the ability to access a variety of photocages with different aniline-pendant ligands.

Reductive amination of **17** with 2-pyridinecarboxaldehyde provides receptor **18**. Subsequent treatment of **18** with the standard reaction sequence affords DiCast-2 containing five nitrogen donor groups. Alternatively, alkylation of **17** with ethyl bromoacetate affords **20**, which was converted to **21** using a synthesis analogous to DiCast-2. Saponification of the ester groups with KOH provides access to DiCast-3. The two carboxylate groups in DiCast-3 provide a charge neutral photocaged complex, which could allow passive loading into cells whereas charged complexes like DiCast-2 may require more invasive techniques to facilitate transport across lipophilic membranes.

Bulk photolysis of MonoCast and DiCast-1 provides the corresponding ligand photoproducts, MonoUnc and DiUnc-1, for use in metal ion binding assays. While the photoproduct of DiCast-2 could be prepared, the photolysis yields an incomplete reaction with the presence of some byproducts that prevent obtaining analytically pure DiUnc-2; however, the purity was deemed sufficient for metal binding assays. In contrast, the apparent decomposition of the DiCast-3 photoproduct made isolating DiUnc-3 impossible.

Metal-Binding Properties of MonoCast and DiCast-1. Titration of DiCast-1 and MonoCast with Cu^{2+}, Zn^{2+}, and Cd^{2+} permits the metal ion binding properties to be evaluated spectrophotometrically. Although ZinCast-1 measurements were also obtained in mixed buffer, the limited water solubility of both new photocages limits the evaluation of metal binding properties to EtOH and CH_3CN. Since Cu^{2+} oxidizes aniline groups in CH_3CN,[22,33] no measurements were made for those conditions. The apo forms of MonoCast and DiCast-1 both possess characteristic, aniline-derived absorption bands with λ_{max} at 260 and 270 nm respectively. Formation of metal complexes of $[M(MonoCast)]^{2+}$ and $[M(DiCast\text{-}1)]^{2+}$ leads to erosion of aniline absorption bands with the simultaneous formation of a new band at ca. 235 nm (Figure 4A). The absorption profiles for both MonoUnc and DiUnc-1 include two bands with λ_{max} at 230 and 350 nm and one band with λ_{min} at ca. 285 nm (Figure 4B). Upon the addition of metal ions, the band at 285 increases in intensity while the other two characteristic features erode. Fitting the absorption changes

dx.doi.org/10.1021/ic400465g | Inorg. Chem. 2013, 52, 8483−8494

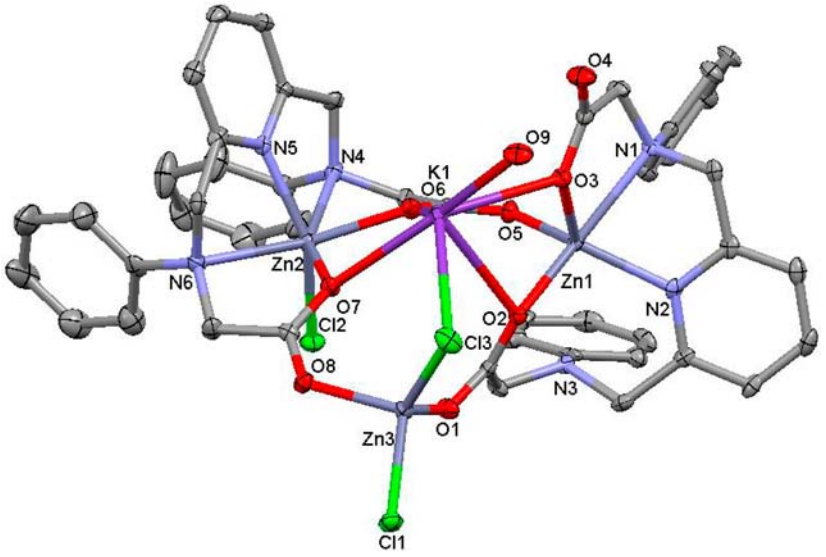

Figure 3. Perspective view of DiCast-3 model complex $[Zn_3K(\mathbf{23})_2(H_2O)Cl_3]$ showing 50% thermal ellipsoids and selected atom labels. Hydrogen atoms are omitted for clarity.

Scheme 2. Synthesis of (A) MonoCast (3) and (B) DiCast-1 (4)

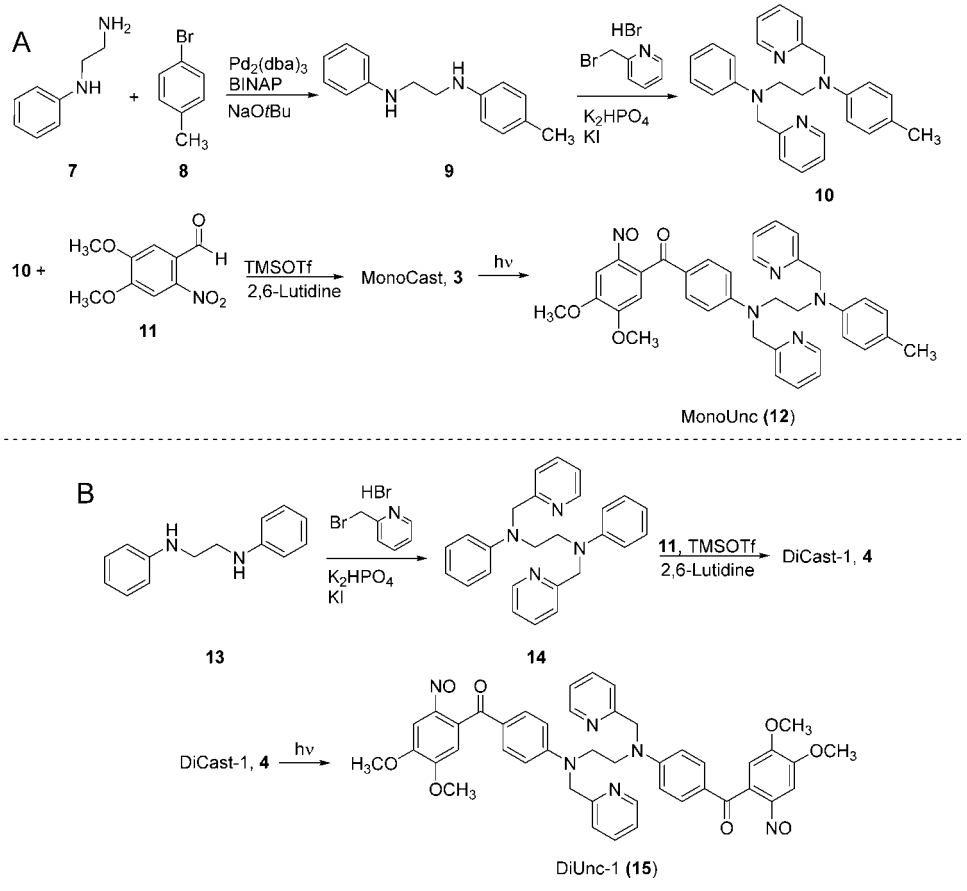

provides apparent binding constants for the respective photocages and photoproducts.

The expansion of the DPA chelator of ZinCast-1 with a second aniline group unexpectedly has a destabilizing effect on the Zn^{2+} complex despite the addition of a fourth pendant ligand. The K_d decreases from 13 μM for $[Zn(ZinCast\text{-}1)]^{2+}$ to 14 μM and 20 μM for $[Zn(MonoCast)]^{2+}$ and $[Zn(DiCast\text{-}1)]^{2+}$ respectively in EtOH (Table 4). The low Zn^{2+} affinity is consistent with replacement of the aliphatic amines in EBAP with aniline groups. The stability of complexes with Cu^{2+} and Cd^{2+} follows a similar trend. In CH_3CN, the affinity of $[Zn(ZinCast\text{-}1)]^{2+}$ (9.7 μM) also exceeds the afinity of $[Zn(MonoCast)]^{2+}$ (12 μM) and $[Zn(DiCast\text{-}1)]^{2+}$ (12 μM). Unlike ZinCast photocages, MonoCast and DiCast-1 exhibit no complex stability dependence on solvent polarity or the metal ion. Stability constants for the $[M(MonoCast)]^{2+}$ and [M-

dx.doi.org/10.1021/ic400465g | Inorg. Chem. 2013, 52, 8483−8494

Scheme 3. Synthesis of (A) DiCast-2 (5) and (B) DiCast-3 (6)

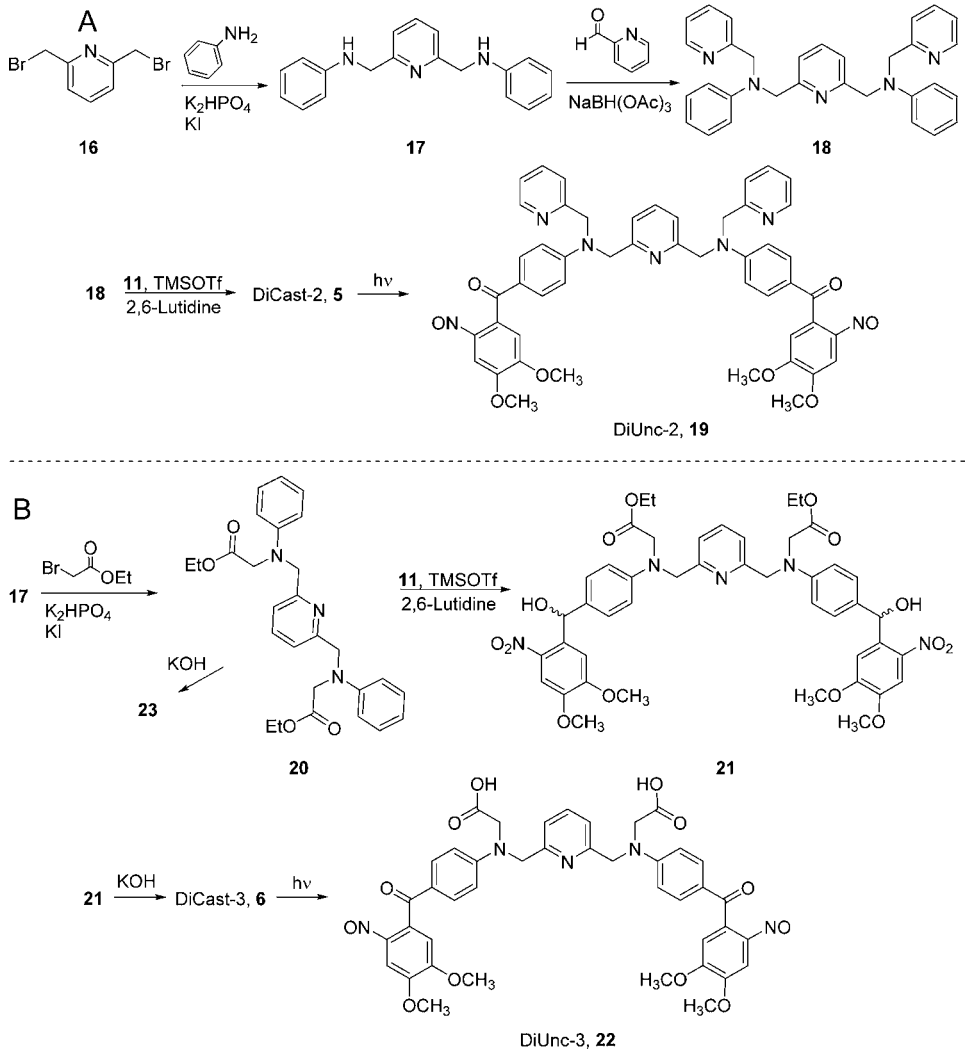

$(DiCast\text{-}1)]^{2+}$ complexes in both solvent systems remain within 14–22 μM, indicating that the second nitrobenzhydrol group has a negligible effect on metal ion affinity of DiCast-1 compared to MonoCast.

The minimal variation in complex stabilities for Cu^{2+} and Zn^{2+} complexes and the ability to accommodate a larger metal ion like Cd^{2+} with comparable affinity suggest increased flexibility in the metal ion receptor. The chelator appears to adopt different conformations easily, which allow metal ions with different coordination requirements to be accommodated readily. The chelator flexibility appears to limit both the selectivity and the affinity, which limits these photocages' biological applications; however, these features are ideal for evaluating properties related to the number of nitrobenzyl groups.

As expected, the resonance interaction between the nitrogen lone pair and the carbonyl oxygen atom introduced upon uncaging decreases the ligand basicity and lowers the affinities measured for the photoproducts. The binding properties of the photoproducts appear to be affected by solvent and metal ion involved (Table 4). Affinities for Zn^{2+} and Cd^{2+} ions are significantly reduced in EtOH compared to CH_3CN, suggesting increased ligand solvation. The stability constants for all photoproduct complexes of $[M(MonoUnc)]^{2+}$ and $[M\text{-}(DiUnc\text{-}1)]^{2+}$ decrease in a pattern that conforms to the Irving–Williams series: $Cu^{2+} > Zn^{2+} > Cd^{2+}$.

The changes in metal affinity after photolysis are more pronounced than the absolute affinity comparisons of the parent photocages. Since uncaging of DiCast-1 modulates the electron density on two metal-bound nitrogen atoms, stability constants for the $[Zn(DiUnc\text{-}1)]^{2+}$ and $[Cd(DiUnc\text{-}1)]^{2+}$ decrease to millimolar values, which leads to significantly larger values for ΔK_d compared to complexes of ZinUnc-1. The 190-fold ΔK_d with Zn^{2+} for DiCast-1 significantly exceeds the 3-fold change determined for ZinCast-1 in EtOH. The 14-fold ΔK_d for MonoCast reflects the trend that weaker binding Cast photocages tend to possess larger ΔK_d values,[14,16] but remains more comparable to the magnitude of change measured for ZinCast-1 than for DiCast-1. DiCast-1 also exhibits a measurable ΔK_d in CH_3CN whereas none was observed for ZinCast-1 or MonoCast. While ΔK_d for DiCast-1 is considerably smaller than the ones measured for Nitr-8 and Nitr-T,[20,31] the measurements demonstrate that larger ΔK_d values can be achieved by introducing a second nitrobenzhydrol group in Cast photocages. The larger ΔK_d values for both [Cd(MonoCast)] and [Cd(DiCast-1)] suggest weaker $N_{aniline}$–M^{2+} bonds. The lack of affinity changes between $[Cu\text{-}(MonoUnc)]^{2+}$ and $[Cu(DiCast\text{-}1)]^{2+}$ indicates the presence

dx.doi.org/10.1021/ic400465g | Inorg. Chem. 2013, 52, 8483–8494

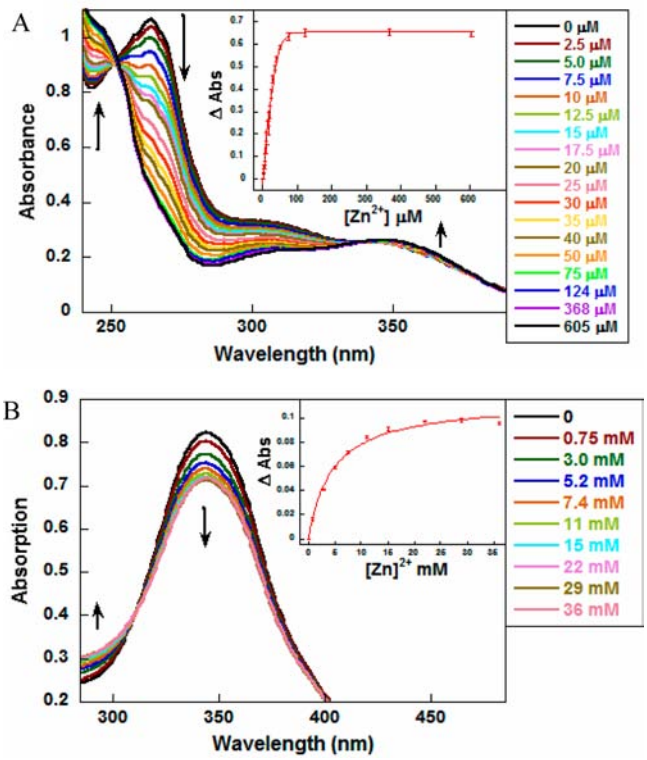

Figure 4. Titration of 25 μM DiCast-1 (top, A) and 15 μM DiUnc-1 (bottom, B) with $Zn(ClO_4)_2$ in EtOH. The absorbance was fitted to a 1:1 binding isotherm (inset). The error bars represent the variance in the measurements over three trials.

of a strong $N_{aniline}-M^{2+}$ interaction imposed by the coordination chemistry of Cu^{2+}, which allows the metal ion to compete more effectively with the resonance interaction for electron density. The trends with Cu^{2+} and Cd^{2+} are consistent with those observed in ZinCast complexes, which were also attributed to differences in aniline–metal ion interactions.[14]

Structural Properties of DiCast-2 and DiCast-3 Receptors. Unlike previous Cast photocages, DiCast-2 and DiCast-3 do not utilize a binding motif directly inspired by a well-known receptor. Analysis of the receptor coordination chemistry can provide important insight into the properties of the corresponding photocage. The modular synthetic strategy allows the receptors to be accessed simultaneously during the photocage synthesis for evaluation. The tripyridine receptor **18** forms a mononuclear distorted trigonal bipyramidal Zn^{2+} complex with a $[Zn(NO_3)_4]^{2-}$ counterion. The three aromatic pyridyl nitrogen atoms define the equatorial plane with the anilino nitrogen atoms in the two axial positions. The $N_{aniline}-Zn-N_{aniline}$ bond angle of the axial groups 157.7(2)° shows significant deviation from the 180° of an ideal trigonal bipyramid. The three equatorial $Zn-N_{Py}$ bond distances occupy a narrow range between 2.002(4) and 2.018(4) Å. The axial nitrogen atoms show modest asymmetry and weaker interactions with $Zn-N_{aniline}$ bond lengths of 2.286(5) Å and 2.271(5) Å. Additional bond angles are consistent with Zn^{2+} coordinating chemistry that allows significant flexibility in the ligand orientations (Table 2).

Receptor **23** exhibits more complicated coordination chemistry in the solid state. Several different structures can be identified crystallographically, but only one refined sufficiently for publication. The reported complex forms a

Table 4. Metal Binding Properties of ZinCast-1,[14] MonoCast, and DiCast-1[a]

		K_d			K_d			K_d		
M^{2+}	solvent	$[M(ZinCast\text{-}1)]^{2+}$	$[M(ZinUnc\text{-}1)]^{2+}$	ΔK_d	$[M(MonoCast)]^{2+}$	$[M(MonoUnc)]^{2+}$	ΔK_d	$[M(DiCast\text{-}1)]^{2+}$	$[M(DiUnc\text{-}1)]^{2+}$	ΔK_d
Zn^{2+}	EtOH	$(1.3 \pm 0.2) \times 10^{-5}$	$(3.5 \pm 0.1) \times 10^{-5}$	3	$(1.4 \pm 0.2) \times 10^{-5}$	$(1.9 \pm 0.1) \times 10^{-4}$	14	$(2.0 \pm 0.3) \times 10^{-5}$	$(3.8 \pm 0.1) \times 10^{-3}$	190
	CH_3CN	$(9.7 \pm 0.4) \times 10^{-6}$	$(9.7 \pm 0.2) \times 10^{-6}$	1	$(1.2 \pm 0.2) \times 10^{-5}$	$(1.4 \pm 0.1) \times 10^{-5}$	1	$(1.2 \pm 0.3) \times 10^{-5}$	$(2.7 \pm 0.1) \times 10^{-5}$	2
Cu^{2+}	EtOH	$(7.2 \pm 0.1) \times 10^{-6}$	$(7.2 \pm 0.3) \times 10^{-6}$	1	$(1.4 \pm 0.1) \times 10^{-5}$	$(1.3 \pm 0.2) \times 10^{-5}$	1	$(1.4 \pm 0.1) \times 10^{-5}$	$(1.5 \pm 0.6) \times 10^{-5}$	1
Cd^{2+}	EtOH	$(1.7 \pm 0.1) \times 10^{-5}$	$(8.2 \pm 0.2) \times 10^{-4}$	48	$(1.5 \pm 0.1) \times 10^{-5}$	$(1.1 \pm 0.1) \times 10^{-3}$	73	$(2.2 \pm 0.3) \times 10^{-5}$	*b*	*b*
	CH_3CN	$(7.9 \pm 0.1) \times 10^{-6}$	$(3.1 \pm 0.1) \times 10^{-5}$	4	$(1.1 \pm 0.1) \times 10^{-5}$	$(2.5 \pm 0.1) \times 10^{-5}$	2	$(1.3 \pm 0.1) \times 10^{-5}$	$(2.9 \pm 0.1) \times 10^{-4}$	22

[a]The 1:1 binding constants were calculated with XLfit. [b]Metal ion affinity was too weak to be accurately determined.

dx.doi.org/10.1021/ic400465g | Inorg. Chem. 2013, 52, 8483–8494

heterobimetallic cluster of two ligands, three Zn^{2+} centers, and one K^+ ion. The cluster forms from the aggregation of two mononuclear Zn^{2+}–receptor complexes that are connected by the K^+ and the third Zn^{2+} site. The K^+ and third Zn^{2+} interact with the two [Zn(**23**)] units through carboxylate ligands that bridge between the internal receptor bound Zn^{2+} centers and these external metal ions. The external Zn^{2+} site is tetrahedral with 2 carboxylate ligands and two Cl^- groups, one terminal and one that bridges to the K^+. The K^+ is formally 7-coordinate, with four carboxylate groups, a water ligand, and two Cl^- groups. The 2 Cl^- ligands bond at approximately 3.1 Å, a distance near the ionic radii sum with K^+, so the interactions are highly electrostatic in nature. The other structures observed contain two [Zn(**23**)] units, and only the external groups and solvent content differ from the reported complex.

The two receptor-bound Zn^{2+} ions adopt different geometries. One Zn^{2+} is octahedral containing the five donor groups from one **23** unit and a Cl^- group in the coordination sphere. The central pyridine and chloride adopt *trans* axial sites with the equatorial sites occupied by the aniline and carboxylate groups that wrap around the metal ion. The Cl–Zn–N_{Py} bond angle of 148.6(1)° illustrates the degree of distortion in the octahedral geometry at the Zn^{2+} site. The aniline nitrogen atoms are *cis* to each other forming a *fac*-like arrangement when including the pyridyl group. The bond lengths and angles are consistent with expected values, but the two Zn–$N_{aniline}$ bond lengths of 2.444(4) Å and 2.503(3) Å are significantly longer that the ones measured in $[Zn(\mathbf{18})]^{2+}$ and exhibit more asymmetry. By comparison the Zn–N_{Py} bonds in the two complexes are nearly identical (Table 3).

The second Zn^{2+} adopts a distorted trigonal bipyramid; however, the fifth ligand comes from a carboxylate ligand that bridges from the Zn^{2+} in the octahedral site. Only one of the two aniline nitrogen ligands in the 5-coordinate site resides within bonding distance to the metal ion. The unbound aniline nitrogen sits at approximately 2.7 Å away from the Zn^{2+} site, whereas the other Zn–$N_{aniline}$ bond length of 2.373(3) Å is the shortest found in the complex of ligand **23**. The $O_{carboxylate}$–Zn–$N_{aniline}$ bond angle (159.1(1)°) that defines the axial sites of the trigonal bipyramid is similar to the geometry found in $[Zn(\mathbf{18})]^{2+}$; however, different ligands define the sites (Table 3).

Metal-Binding Properties of DiCast-2 and DiCast-3. In addition to evaluating the binding properties of DiCast-2 and DiCast-3 under the same conditions as Dicast-1, DiCast-3 possesses sufficient solubility to conduct measurements under simulated physiological conditions (50 mM HEPES, 100 mM KCl, pH 7). The spectroscopic profiles of DiCast-2 and DiCast-3 exhibit the same features as DiCast-1 with an aniline-derived charge transfer band with λ_{max} at 260 nm that decreases in intensity upon the addition of metal ions (Figure 5A). The analogous blue-shifted λ_{max} absorption band that forms upon metal ion binding appears at shorter wavelengths than that of DiCast-1 and outside of the instrument's detection limit (Figure 5B). The inclusion of the third pyridine increases the Zn^{2+} affinity of DiCast-2 to 8.7 μM as measured in EtOH (Table 5). The replacement of pyridine ligands with carboxylate group further enhances the Zn^{2+} K_d of DiCast-3 to 5.0 μM. Similar modest increases in binding affinity occur for both photocages in CH_3CN. The trends in increased affinity between the DiCast-1 and the second generation photocages also persist in the measurements with Cu^{2+} and Cd^{2+}.

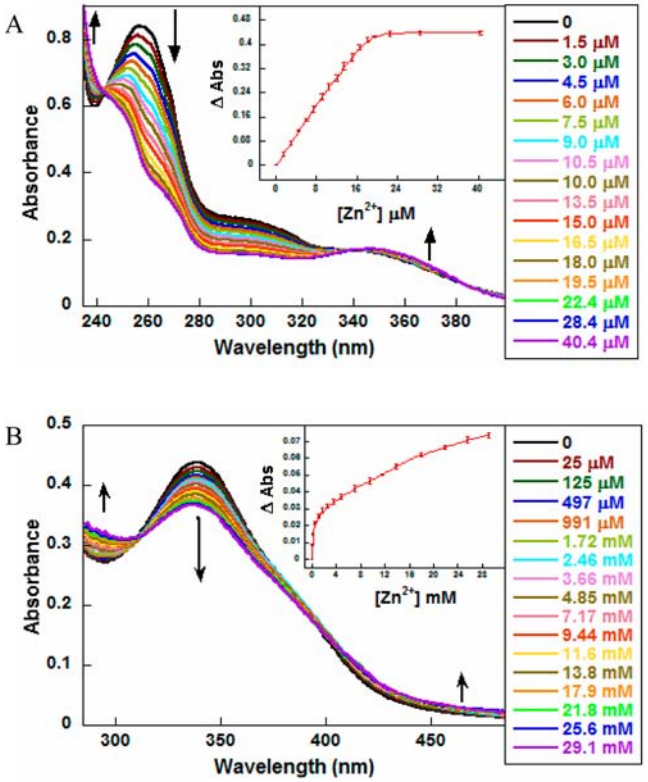

Figure 5. Titration of 25 μM DiCast-2 (top, A) and DiUnc-2 (bottom, B) with $Zn(ClO_4)_2$ in EtOH. The absorbance was fitted to a 1:1 binding isotherm (inset). The error bars represent the variance in the measurements over three trials.

Limited access to the uncaged photoproducts limits quantitative analysis of binding affinity and ΔK_d to DiCast-2. The K_d for $[Zn(DiUnc\text{-}2)]^{2+}$ (4.2 mM) and $[Zn(DiUnc\text{-}1)]^{2+}$ (3.8 mM) are nearly identical, but the ΔK_d more than doubles because of the increased affinity of the DiCast-2 photocage. The 480-fold ΔK_d exceeds all the Cast derivatives investigated to date. Based on the solvent-dependent affinity trends observed in Cast photocages,[14] the ΔK_d would be larger if DiCast-2 could be evaluated in aqueous solution. Lack of access to DiUnc-3 prevented quantification of metal ion binding, but qualitative results suggest that the photoproduct binds more weakly than the parent photocage. Based on the analysis of the Zn^{2+} model complex, however, we hypothesize that the ΔK_d for DiCast-3 would be smaller than for DiCast-2. The distinct asymmetry of the $N_{aniline}$–Zn bond lengths suggests an unequal contribution of these ligands to the overall complex stability.

The DiCast-2 affinity measurements reinforce the conclusions from the ZinCast and CrownCast series. The use of aniline ligands inherently limits the magnitude of the absolute binding affinity. Even using a well-defined binding pocket and increasing denticity fails to overcome the use of weakly coordinating aromatic nitrogen ligands. When stronger binding ligands are incorporated into an aniline-based Cast receptor, these ligands dominate metal ion binding and attenuating the electron density on the anilino nitrogen atom has minimal effects on complex stability.

■ CONCLUSION

The inclusion of two nitrobenzyl groups in a Zn^{2+} photocage increases the ΔK_d by at least an order of magnitude compared

dx.doi.org/10.1021/ic400465g | Inorg. Chem. 2013, 52, 8483–8494

Table 5. Metal Binding Properties of DiCast-2 and DiCast-3[a]

		K_d			K_d	
M^{2+}	solvent	$[M(DiCast\text{-}2)]^{2+}$	$[M(DiUnc\text{-}2)]^{2+}$	ΔK_d	$[M(DiCast\text{-}3)]^{2+}$	$[M(DiUnc\text{-}3)]^{2+}$
Zn^{2+}	EtOH	$(8.7 \pm 0.3) \times 10^{-6}$	$(4.2 \pm 0.4) \times 10^{-3}$	480	$(5.0 \pm 0.3) \times 10^{-6}$	*b*
	CH_3CN	$(1.0 \pm 0.5) \times 10^{-5}$	$(3.3 \pm 0.2) \times 10^{-3}$	330	$(7.8 \pm 0.8) \times 10^{-6}$	*b*
	buffer[d]	*c*	*c*		$(7.8 \pm 0.7) \times 10^{-6}$	*b*
Cu^{2+}	EtOH	$(8.6 \pm 0.3) \times 10^{-6}$	$(1.1 \pm 0.8) \times 10^{-6}$	2	$(6.9 \pm 0.3) \times 10^{-6}$	*b*
	buffer	*c*	*c*		$(7.3 \pm 0.3) \times 10^{-6}$	*b*
Cd^{2+}	EtOH	$(9.5 \pm 0.5) \times 10^{-6}$	$(\sim 1.0 \pm 0.2) \times 10^{-3}$	110	$(8.2 \pm 0.7) \times 10^{-6}$	*b*
	CH_3CN	$(8.5 \pm 0.5) \times 10^{-6}$	$(\sim 9.3 \pm 0.1) \times 10^{-4}$	110	$(9.3 \pm 0.3) \times 10^{-6}$	*b*
	buffer[d]	*c*	*c*		$(1.2 \pm 0.1) \times 10^{-5}$	*b*

[a]The 1:1 binding constants were calculated with XLfit. [b]DiUnc-3 of sufficient purity could not be isolated. [c]Metal affinity was not determined due to low solubility of the complex. [d]50 mM HEPES, 100 mM KCl, pH 7.

to the analogous monofunctionalized compounds. The results obtained for all three DiCast Zn^{2+} photocages are consistent with trends observed in similar Ca^{2+} systems. Both difunctional Ca^{2+} photocages utilize an identical metal ion receptor, whereas we have screened several different, yet related, binding motifs in this investigation. While the DiCast photocages exhibit significant improvement over the ZinCast precursors, several aspects related to the complex design will probably limit the biological application of these photochemical tools.

The dependence on Cast photocages on aniline-based ligands minimizes the absolute Zn^{2+} affinity attainable unless tightly binding ligands are added to the chelator, which significantly decreases the ΔK_d. The DiCast photocages would be useful for introducing Zn^{2+} into biological systems with μM basal Zn^{2+} level; however, the complexes would perturb homeostasis mechanisms prior to photolysis in most cells where $[Zn^{2+}]$ are tightly regulated. The general strategy utilized by DiCast photocages may be more applicable to investigations of other biologically relevant metal ions that are present at higher concentrations.

In addition to metal ion buffering considerations, the nitrobenzylhydrol−aniline receptor strategy has problems associated with the efficiency of the nitrobenzyl photochemistry. The Cast photocages exhibit low quantum yields,[14,23] which are exacerbated in the DiCast compounds as evidenced by the bulk synthesis of the photoproducts. Incomplete photoreactions and instability of some photoproducts make accurately calculating changes in metal ion concentrations difficult. Finding a suitable replacement for the nitrobenzyl photocaging group is a high priority of our current research. Despite the possible limitations for studying Zn^{2+}, the findings significantly increase the understanding of multifunctional photocaged complexes and will help facilitate the design of future tools for studying metal ion homeostasis.

■ ASSOCIATED CONTENT

Supporting Information

Figures showing metal ion titrations for MonoCast, DiCast-1, DiCast-2, and DiCast-3. Figures showing the ^1H and ^{13}C NMR spectra for all new compounds synthesized. Additional X-ray data and fully labeled X-ray structures of $[Zn(\mathbf{18})][Zn(NO_3)_4]$ and $[Zn_3K(\mathbf{23})_2(H_2O)Cl_3]$. CIF files for $[Zn(\mathbf{18})][Zn(NO_3)_4]$ and $[Zn_3K(\mathbf{23})_2(H_2O)Cl_3]$. This material is available free of charge via the Internet at http://pubs.acs.org.

■ AUTHOR INFORMATION

Corresponding Author

*E-mail: scburdette@wpi.edu. Tel: (508) 831-5224.

Notes

The authors declare no competing financial interest.

■ ACKNOWLEDGMENTS

The work was funded by Worcester Polytechnic Institute and by NSF Grant CHE-0955361.

■ REFERENCES

(1) Yu, H.; Li, J.; Wu, D.; Qiu, Z.; Zhang, Y. *Chem. Soc. Rev.* **2010**, *39*, 464−473.
(2) Ellis-Davies, G. C. *Chem. Rev.* **2008**, *108*, 1603−1613.
(3) Ciesienski, K. L.; Franz, K. J. *Angew. Chem., Int. Ed.* **2011**, *50*, 814−824.
(4) Adams, S. R.; Tsien, R. Y. *Annu. Rev. Physiol.* **1993**, *55*, 755−784.
(5) Gwizdala, C.; Burdette, S. C. *Curr. Opin. Chem. Biol.* **2013**, *17*, 137−142.
(6) Mbatia, H. W.; Burdette, S. C. *Biochemistry* **2012**, *51*, 7212−7224.
(7) Bitanihirwe, B. K.; Cunningham, M. G. *Synapse* **2009**, *63*, 1029−1049.
(8) Paoletti, P.; Vergnano, A.; Barbour, B.; Casado, M. *Neuroscience* **2009**, *158*, 126−136.
(9) Barnham, K. J.; Bush, A. I. *Curr. Opin. Chem. Biol.* **2008**, *12*, 222−228.
(10) Kepp, K. P. *Chem. Rev.* **2012**, *112*, 5193−5239.
(11) Bandara, H.; Walsh, T. P.; Burdette, S. C. *Chem.—Eur. J.* **2011**, *17*, 3932−3941.
(12) Bandara, H. D.; Kennedy, D. P.; Akin, E.; Incarvito, C. D.; Burdette, S. C. *Inorg. Chem.* **2009**, *48*, 8445−8455.
(13) Gwizdala, C.; Kennedy, D. P.; Burdette, S. C. *Chem. Commun.* **2009**, 6967−6969.
(14) Gwizdala, C.; Singh, C. V.; Friss, T. R.; MacDonald, J. C.; Burdette, S. C. *Dalton Trans.* **2012**, *41*, 8162−8174.
(15) Kennedy, D. P.; Gwizdala, C.; Burdette, S. C. *Org. Lett.* **2009**, *11*, 2587−2590.
(16) Mbatia, H. W.; Kennedy, D. P.; Camire, C. E.; Incarvito, C. D.; Burdette, S. C. *Eur. J. Inorg. Chem.* **2010**, *2010*, 5069−5078.
(17) Colvin, R. A.; Holmes, W. R.; Fontaine, C. P.; Maret, W. *Metallomics* **2010**, *2*, 306−317.
(18) Kantevari, S.; Narasimhaji, C. V.; Mereyala, H. B. *Tetrahedron* **2005**, *61*, 5849−5854.
(19) Omran, Z.; Specht, A. *J. Photochem. Photobiol., A* **2009**, *208*, 125−130.
(20) Cui, J.; Gropeanu, R. A.; Stevens, D. R.; Rettig, J.; del Campo, A. *J. Am. Chem. Soc.* **2012**, *134*, 7733−7740.
(21) Mbatia, H. W.; Kennedy, D. P.; Burdette, S. C. *Photochem. Photobiol.* **2012**, *88*, 844−850.
(22) Kennedy, D. P.; Incarvito, C. D.; Burdette, S. C. *Inorg. Chem.* **2010**, *49*, 916−923.
(23) Kennedy, D. P.; Brown, D. C.; Burdette, S. C. *Org. Lett.* **2010**, *12*, 4486−4489.
(24) Caputo, C. A.; Price, J. T.; Jennings, M. C.; McDonald, R.; Jones, N. D. *Dalton Trans.* **2008**, 3461−3469.

(25) Pohlke, R.; Fischer, W. Process for the preparation of alkylene-bis (2-pyridylamine) compounds and Karl Fischer reagents and methods utilizing such compounds. US Patent No. 5,086,000, 1992.
(26) Katritzky, A. R.; Fan, W.; Fu, C. *J. Org. Chem.* **1990**, *55*, 3209−3213.
(27) Liu, P.; Chen, Y.; Deng, J.; Tu, Y. *Synthesis* **2001**, *2001*, 2078−2080.
(28) *XLfit, 5.1.0.0*; ID Business Solutions Limited: Guildford, U.K., 2009.
(29) *Bruker SAINT 6.14 and SHELXTL 6.14 for WNT/2003*; Bruker AXS Inc.: Madison, WI, 1999.
(30) Yamada, M.; Kondo, M.; Miyasato, R.; Naka, Y.; Mamiya, J.; Kinoshita, M.; Shishido, A.; Yu, Y.; Barrett, C. J.; Ikeda, T. *J. Mater. Chem.* **2009**, *19*, 60−62.
(31) Adams, S.; Kao, J. P.; Grynkiewicz, G.; Minta, A.; Tsien, R. *J. Am. Chem. Soc.* **1988**, *110*, 3212−3220.
(32) Melton, D. L.; VanDerveer, D. G.; Hancock, R. D. *Inorg. Chem.* **2006**, *45*, 9306−9314.
(33) Kirchgessner, M.; Sreenath, K.; Gopidas, K. R. *J. Org. Chem.* **2006**, *71*, 9849−9852.